

Chapter 4

Spatiotemporal Pattern Formation in Neural Fields with Linear Adaptation

G. Bard Ermentrout, Stefanos E. Folias, and Zachary P. Kilpatrick

Abstract We study spatiotemporal patterns of activity that emerge in neural fields

waves [27, 53], suggesting that some process other than inhibition must curtail

system [26, 54]. This single stationary “bump” can be perturbed and pinned with external stimuli as we see in subsequent sections of this chapter.

4.2.1.2 Imaginary Eigenvalues

When τ (strong or slow adaptation), then the trace vanishes at a lower critical value than the determinant. Let τ^*

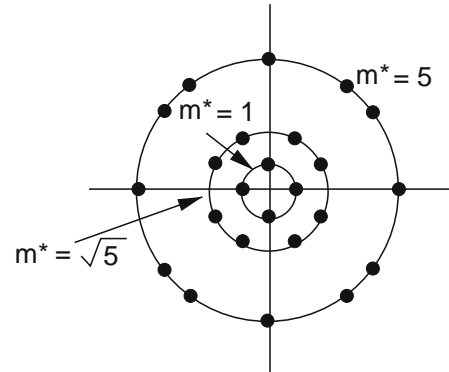
Fig. 4.2 Three different cases of critical wavenumbers in the square lattice. The critical wavenumbers are (from out to in),

$$\left\{ \pm \begin{matrix} \pm \\ \pm \end{matrix} \right\},$$

$$\left\{ \pm \begin{matrix} \pm & - \\ \pm & - \end{matrix} \right\},$$

and

$$\left\{ \begin{matrix} \pm & \pm \\ \pm & \pm \end{matrix} \right\}, \left\{ \begin{matrix} \pm & - \\ \pm & - \end{matrix} \right\}, \left\{ \begin{matrix} \pm & \pm \\ \pm & - \end{matrix} \right\}, \left\{ \begin{matrix} \pm & - \\ \pm & \pm \end{matrix} \right\},$$



see only stable traveling waves. Figure 4.1

nonzero solutions, $z_1 = z_2 = z_3 = z_4 = \dots$ which are stable if $\{ \dots \}$. We remark that the triplet solutions $z_1 = z_2 = z_3 = \dots$ are never stable and that if $\dots =$

cycles along the principle directions. In the simulations illustrated in the figure, we change u_1 .

4.3 Response to Inputs in the Ring Network

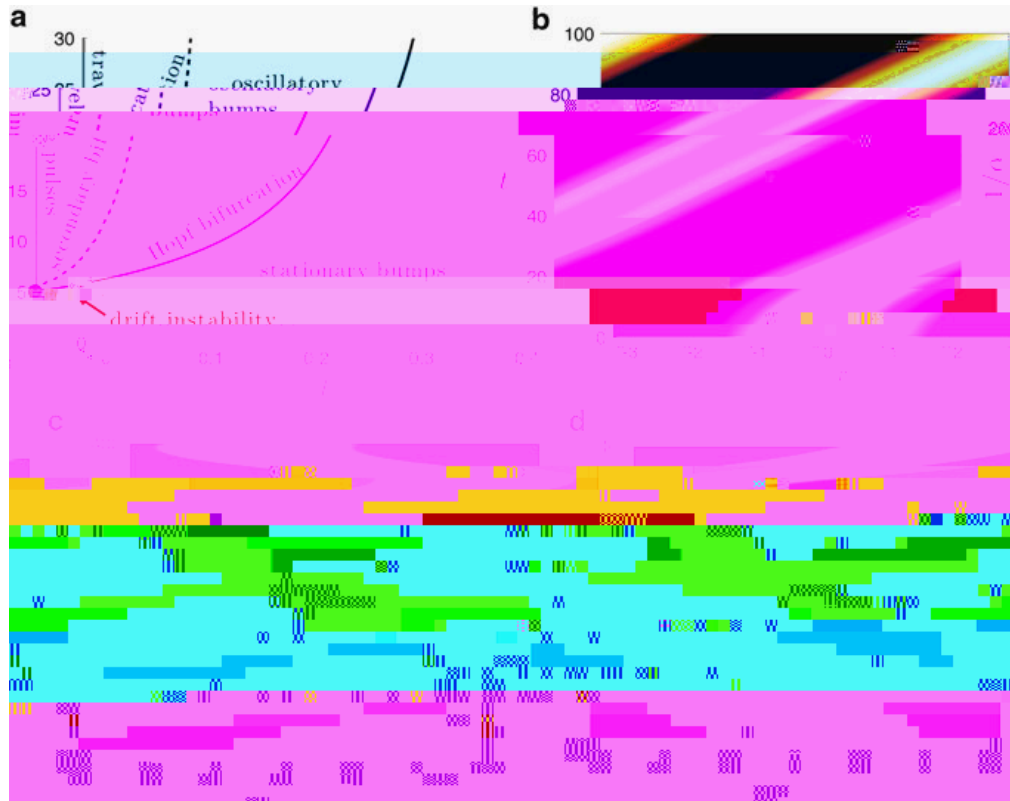


Fig. 4.4 (a) Partition of (l, α) parameter space into different dynamical behaviors of the bump solution (4.12) for Heaviside firing rate (4.8). Numerical simulation of the (

a moving input is introduced, the system tends to lock to it if it has speed commensurate with that of the natural wave. Converting to a wave coordinate frame $\xi = x - ct$, where we choose the stimulus speed c , we can study traveling wave solutions $u(\xi, t) = U(\xi)$ of (4.1)

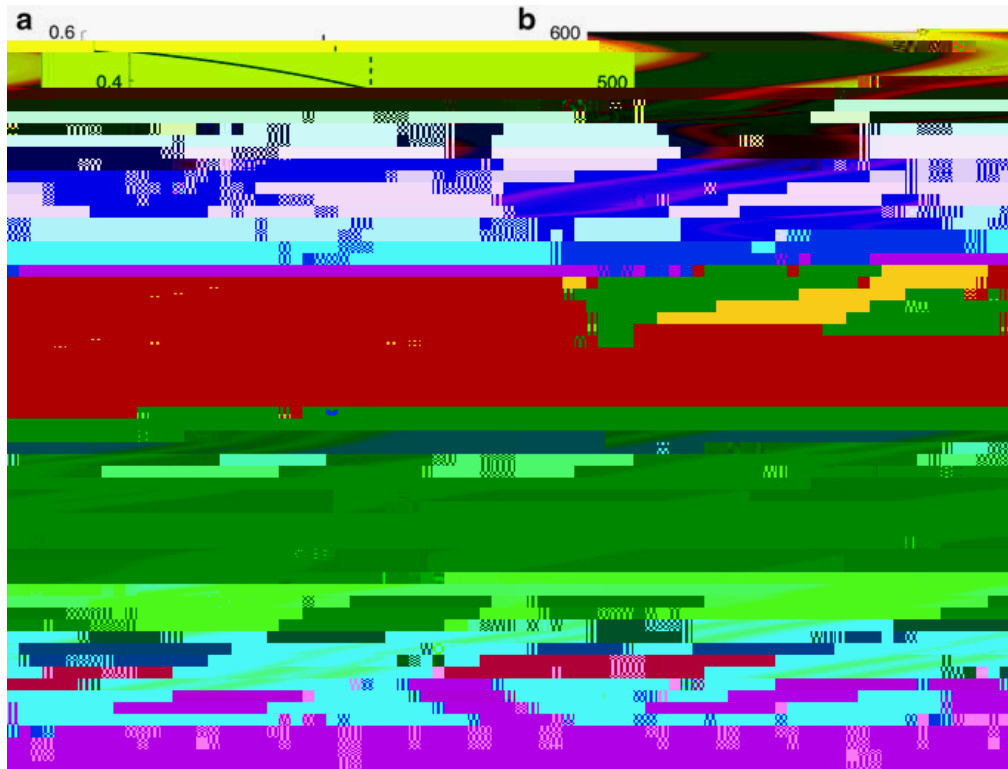


Fig. 4.5 Sloshing instability of stimulus-locked traveling bumps (4.33) in adaptive neural field (4.1) with Heaviside firing rate (4.8). **(a)** Dependence of stimulus locked pulse width Δ on stimulus speed v_s , calculated using the implicit equations (4.36) and (4.37). **(a)** Zeros of the Evans function $E = \det A_\Delta - I$, with (4.47), occur at the crossings of the zero contours of $\text{Re}E$ (black) and $\text{Im}E$ (grey). Presented here for stimulus speed $v_s = v_c$, just beyond the Hopf bifurcation at $v_s \approx v_c$. Breathing instability occurs in numerical simulations for **(b)**, $v_s = v_c$ and **(c)**, $v_s = v_c$. **(d)** When stimulus speed $v_s = v_c$ is sufficiently fast, stable traveling bumps lock. Other parameters are $\tau = 1$, $\alpha = 1$, $\beta = 1$, and $\gamma = 1$.

$$A_\Delta =$$

function (4.8). In parameter regime we show, there are two pulses for each parameter value, either both are unstable or one is stable. As the speed of stimuli is decreased, a stable traveling bump undergoes a Hopf bifurcation. For sufficiently fast stimuli, a stable traveling bump can lock to the stimulus, as shown in Fig. 4.5d. However, for

$$U_0(x)$$



dynamics of the adaptation variable ν additionally governs the stability of the stationary bump [22]. In particular, if $\alpha < \beta$, stationary bumps are always unstable. Stable bumps in the scalar model of Amari can extend to this model only for $\alpha > \beta$, and a stable bump for $\alpha > \beta$ destabilizes as α decreases through $\alpha = \beta$ leading to a drift instability [22] that gives rise to traveling bumps.

CASE II: Localized Excitatory Input $\nu = \nu_0 + \tilde{\nu}$. A variety of bifurcation scenarios can occur [22, 23], and, importantly, stationary bumps can emerge in a saddle-node bifurcation for strong inputs in parameter regimes where stationary bumps do not exist for weak or zero input as shown in Fig. 4.6. When stationary bumps exist for $\alpha > \beta$, the stability of a bump is determined directly by the geometry of the bifurcation curves [22, 23] (e.g., see Fig. 4.6). As α decreases through $\alpha = \beta$, a Hopf bifurcation point emerges from a saddle-node bifurcation point (associated with the sum mode Ω_c) and destabilizes a segment of a branch of stable bumps for $\alpha > \beta$. Generally, Hopf bifurcations occur with respect to either of two spatial modes Ω (discussed later), and their relative positions (denoted by \oplus and \ominus , respectively, on the bifurcation curves in Fig. 4.6) can switch depending on parameters [22].

Stability of Stationary Bumps. By setting $u = u_0 + \tilde{u}$ and $\nu = \nu_0 + \tilde{\nu}$, we study the evolution of small perturbations $\tilde{u}, \tilde{\nu}^T$ in a Taylor expansion of (4.1) about the stationary bump $(u_0, \nu_0)^T$. To first order in $\tilde{u}, \tilde{\nu}^T$, the perturbations are governed by the linearization

$$\begin{aligned} \dot{\tilde{u}} &= -\tilde{u} - \beta \tilde{\nu} & w &= \int_0^\infty (u_0 - \nu) \\ \dot{\tilde{\nu}} &= \alpha \tilde{u} - \tilde{\nu} & & \end{aligned} \quad / \epsilon$$

and $\tilde{u} = \sum \tilde{u}_k$ in (4.52)

where $\tilde{u}^T \in \mathbb{R}^n$ denoting uniformly continuously differentiable vector-valued functions $\mathbf{u} : \mathbb{R} \rightarrow \mathbb{R}^n$. This leads to the spectral problem for $\tilde{u}, \tilde{\nu}^T$

$$\begin{pmatrix} \lambda & 0 \\ 0 & \lambda \end{pmatrix} \begin{pmatrix} \tilde{u} \\ \tilde{\nu} \end{pmatrix} = \begin{pmatrix} -1 & -\beta \\ \alpha & -1 \end{pmatrix} \begin{pmatrix} \tilde{u} \\ \tilde{\nu} \end{pmatrix} + \mathcal{N} \begin{pmatrix} \tilde{u} \\ \tilde{\nu} \end{pmatrix} \quad (4.53)$$

where $\mathcal{N} \begin{pmatrix} \tilde{u} \\ \tilde{\nu} \end{pmatrix} = \int_0^\infty w \tilde{u} - \tilde{\nu} \tilde{u}$

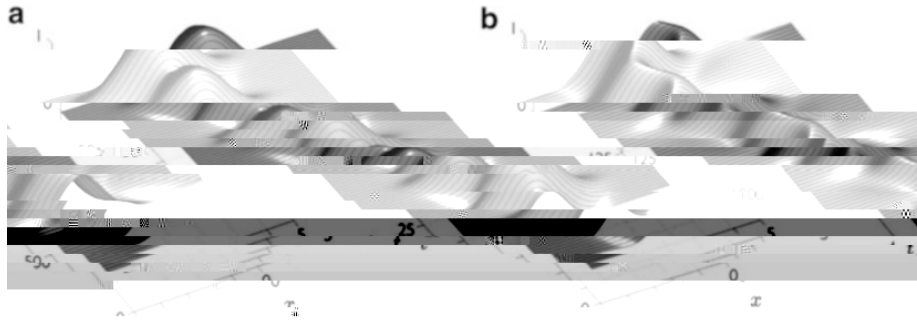
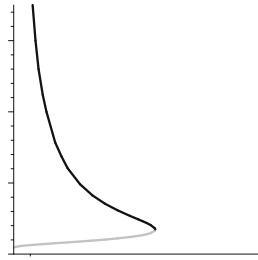


Fig. 4.7 Destabilization of spatial modes Ω_{C_1} and Ω_{C_2} , as the bifurcation parameter μ_1 is varied through a Hopf bifurcation, can give rise to a stable *breather* or *slosher*, respectively, depending on the relative position of the bifurcation points for each spatial mode (e.g., μ_{C_1} and μ_{C_2} , Fig. 4.6c). **(a)** a plot of u_{C_1} exhibiting a breather arising from destabilization of the sum mode Ω_{C_1} for $\mu_1 = 0.5$, $\bar{w} = 0.5$, $\beta = 0.5$, $\alpha = 0.5$, $\gamma = 0.5$. **(b)** a plot of u_{C_2} exhibiting a slosher arising from destabilization of the difference mode Ω_{C_2} for $\mu_1 = 0.5$, $\bar{w} = 0.5$, $\beta = 0.5$, $\alpha = 0.5$, $\gamma = 0.5$. Common parameters: $\epsilon = 0.01$, $\bar{w}_0 = 0.5$, $\mu_0 = 0.5$.

the two threshold crossings of the bump relative to the position of the input $I(x)$. This results in consistency conditions for the existence of a *stimulus-locked* traveling bump:

$$\begin{aligned}
 x_1 &= x_0 - \mathcal{M}_C(x_1 - x_0) - c \mathcal{M}(x_1) \\
 x_2 &= x_1 - \mathcal{M}_C(x_2 - x_1) - c \mathcal{M}(x_2)
 \end{aligned}$$



Stability of Traveling Bumps. By setting $u = u_0 + \tilde{u}$ and $v = v_0 + \tilde{v}$, we study the evolution of small perturbations $(\tilde{u}, \tilde{v})^T$ in the linearization of (4.1) about the

15. Dionne, B., Silber, M., Skeldon, A.C.: Stability results for steady, spatially periodic planforms. *Nonlinearity* **10**, 321 (1997)
16. Ermentrout, B.: Stripes or spots? Nonlinear effects in bifurcation of reaction-diffusion equations on the square. *Proc. R. Soc. Lond. Ser. A: Math. Phys. Sci.* **434**(1891), 413–417 (1991)
17. Ermentrout, B.: Neural networks as spatio-temporal pattern-forming systems. *Rep. Prog. Phys.* **61**, 353–430 (1998)
18. Ermentrout, G.B., Cowan, J.D.: A mathematical theory of visual hallucination patterns. *Biol. Cybern.* **34**(3), 137–150 (1979)
19. Ermentrout, G.B., Cowan, J.D.: Secondary bifurcation in neuronal nets. *SIAM J. Appl. Math.* **39**(2), 323–340 (1980)

